JOURNAL OF MATERIALS SCIENCE 26 (1991) 4678–4682

Laser–arc hardening of aluminium alloys

D. M. GUREYEV, A. V. ZOLOTAREVSKY, A. E. ZAIKIN
P. N. Lebedev Physical Institute, USSR Academy of Sciences, Kuibyshev Branch, Kuibyshev, USSR

The characteristics of a joint laser–arc hardening of the aluminium alloys V124 and Al25 are investigated. Optimum parameters for the process are established. The laser–arc source gives a greater hardening effect in comparison with that of the arc source at treatment rates over 17 mm s. A microstructural analysis of the solidified melt zone showed that it represents α-phase dendrites surrounded by the eutectic Al–Si in which silicon has a fibre structure. With the aid of quantitative metallography, the parameters of the melt crystallization are determined for the case of fusion by the laser–arc source.

1. Introduction

Recent investigations have shown that the local fusion of a thin surface layer by means of concentrated energy sources is an efficient method of hardening different materials, including aluminium alloys. As a rule, laser radiation is used as the energy source. In the majority of cases, the use of combined sources joining the laser radiation effect with the arc discharge plasma is more efficient and more economical. Such energy sources have already been applied in cutting and welding [1]. Their application is also justified for the hardening of aluminium alloys: their low absorption capacity, especially for laser radiation with a wavelength of 10.6 μm, and their high thermal conductivity puts certain limits on the choice of possible laser sources. In this paper the peculiarities of the laser–arc hardening of aluminium alloys are analysed.

2. Experimental procedure

It is known from the literature on laser hardening [2] that the maximum effect of hardening in the case of aluminium alloys is achieved for eutectic and post-eutectic alloys of the type Al–Si. For our investigations, the alloys Al25 and V124 were chosen; their composition is presented in Table I. The treatment was carried out at two stations. The first was a welding source VSVU-80, a CO_2-laser LGN-702 with the exit power of radiation $P = 500$ W ($q = 5 \times 10^5$ W cm^{-2}) and a coordinate bench with a linear velocity of movement up to 7 mm s^{-1}. At this station, rectangular samples of $12 \times 30 \times 40$ mm were treated. The treatment at linear velocities of movement over 8 mm s^{-1} was carried out at the second stand consisting of the same welding source VSVU-80, CO_2-laser LATUS-31 with exit power of radiation $P = 1000$ W ($q = 1.3 \times 10^5$ W cm^{-2}) and devices for the rotation of the samples with frequency from 1 to 50 revs min^{-1}. Cylindrical samples of 100-mm diameter were treated at the second station.

In both cases, the tungsten electrode of the welding head was conveyed to the zone of the laser-beam effect at an angle of 45° with respect to its axis (Fig. 1). The electrode diameter was 3 mm, the gap between the electrode and the sample ~ 1 mm, and its shift with respect to the laser spot was 1–2 mm. The electrode was a cathode, and the sample an anode. The zone under treatment was blown by argon, at a flow rate of 8 l min^{-1}.

The structure of the arc-supported laser-effect zone was investigated by means of optical microscopy and transmission and scanning electron microscopy. The microhardness and size of the fused layer were measured with the aid of a PMT-3 device. Quantitative metallography was performed by Epiquant (Karl Zeiss, Jena, Germany).

3. Results and discussion

3.1. Microstructure and crystallization parameters

After the combined laser–arc treatment at the surface of the samples, a layer hardened from the liquid state is formed, its microhardness 1.5–1.8 times higher than the microhardness of the initial material. The microstructure is also significantly changed (Fig. 2). Before

TABLE I Composition of aluminium alloys V124 and Al25 and the result of their microhardness H_{50} change after laser–arc treatment

Alloy	Si (%)	Cu (%)	Mg (%)	Mn (%)	Ti (%)	Ni (%)	Fe (%)	H_{50} (kg mm^{-2}) initial	hardened
V124	8–11	3–4	0.15–0.35	0.1–0.3	0.1–0.3	–	0.3	90	135–165
Al25	11–13	1.5–3.0	0.8–1.3	0.3–0.6	0.05–0.20	0.8–1.3	0.8	88	130–155

0022–2461/91 $03.00 + .12

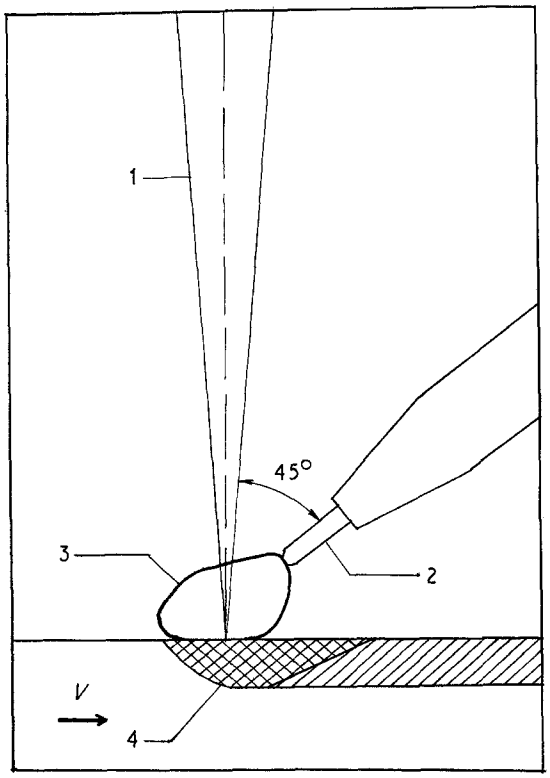

Figure 1 Scheme of the arc-supported laser treatment. 1, Laser beam; 2, tungsten electrode; 3, plasma of arc discharge; 4, melted zone.

treatment, the structures of the alloys V124 and Al25, were different. The alloy Al25, in contrast to the alloy V124, is modified during casting and therefore in the plane of the microsection rounded and more dispersed silicon crystals are observed. After the arc-supported laser fusion, the microstructures of the alloys become almost identical and are dendrites of the α-phase (a solid solution on the base of Al), surrounded by the eutectic Al–Si. The α-phase percentage by volume, measured by the installation Epiquant, ranged from 30 to 60 vol %, which proves the shift of the eutectic point in the direction of greater concentrations of silicon. The α-phase dendrites have the same orientation in the boundaries of one grain. Such grains are well defined at the longitudinal microsection (along the melted zone). In this case, the dendrites in the grains adjoining the bottom of the melted zone are perpendicular to the surface. As the distance from the bottom is increasing, the direction of dendrite growth is changed and becomes practically parallel to the surface in the upper layer (Fig. 3).

By assuming that the dendrites are growing in the direction of the maximum heat removed, one may estimate their rate of growth, R [3]

$$R = v \cos\theta \qquad (1)$$

where v is the linear velocity of the sample movement

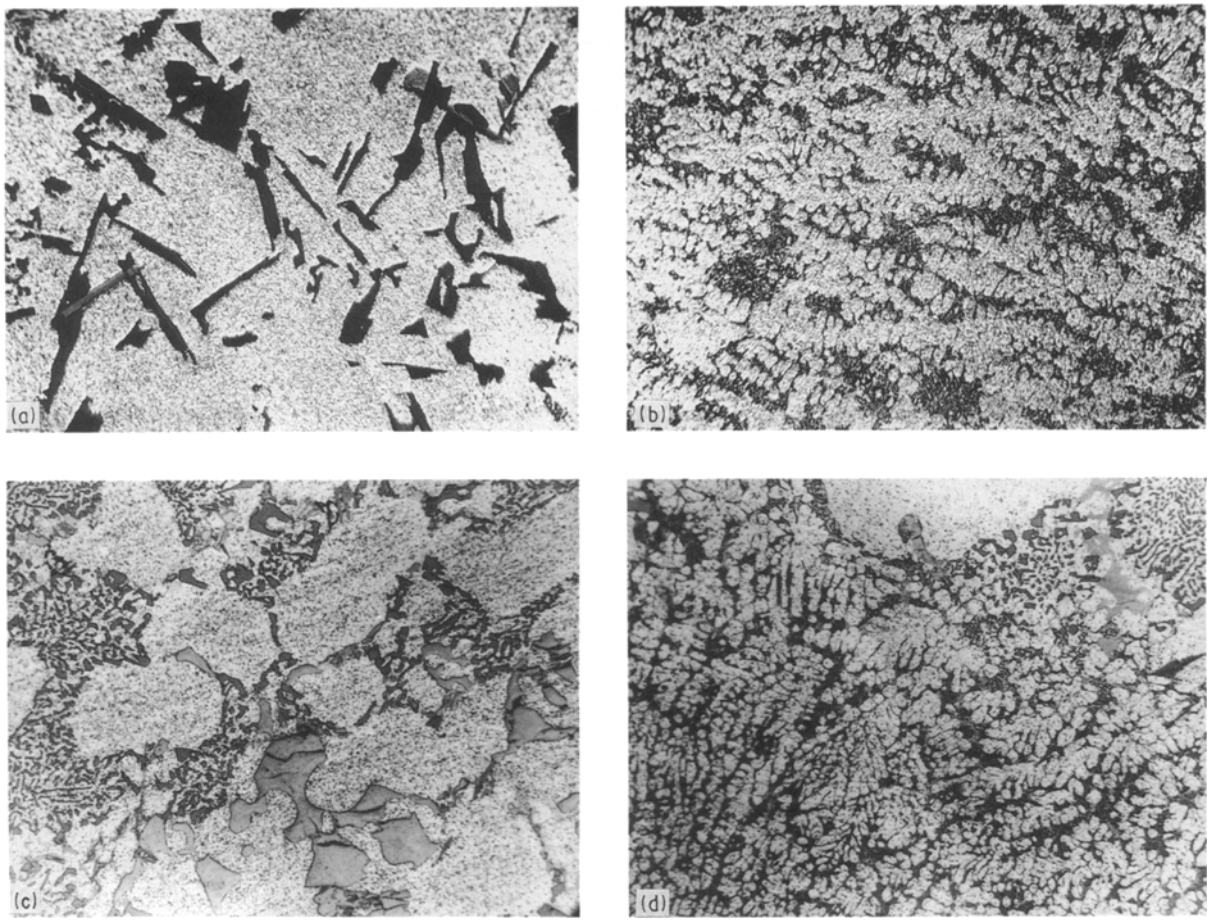

Figure 2 Microstructure of the alloys V124 (a, b) and Al25 (c, d) before (a, c) and after (b, d) the laser–arc treatment.

TABLE II Measurements of the interdendrite distance λ and calculation of the cooling rates, W, at the crystallization front, dendrite growth rates, R, and temperature gradient, G, for the aluminium alloy Al25 subjected to laser–arc treatment

Location in solidified melt zone	λ (μm)	W (K s^{-1})	R (mm s^{-1})	G (K mm^{-1})	Laser–arc treatment parameters			
					v (mm s^{-1})	q (W cm^{-2})	I (A)	IU (kW)
Surface	2.5	7.1×10^3	6.9	1.0×10^3				
Middle	3.1	3.7×10^3	4.5	0.8×10^3	7.0	5×10^5	70	1.0
Bottom	3.6	2.5×10^3	–	–				

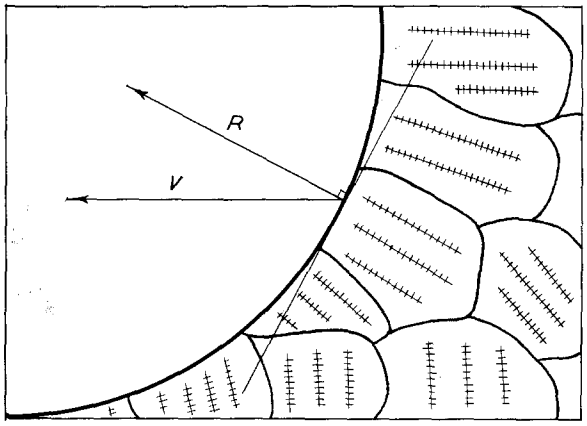

Figure 3 Scheme of α-phase dendrite growth in the melted zone (longitudinal section).

and θ the angle of direction of the main axis of the dendrites with the direction of movement. The rate of cooling, W, at the crystallization front is estimated by a known equation relating the rate of cooling to the distance between the axes of the secondary dendrites, λ

$$\lambda = A\, W^{-n} \quad (2)$$

$$W = \mathrm{d}T/\mathrm{d}t = R\, G \quad (3)$$

where G is the temperature gradient, and A and n are constant coefficients. Thus for the alloys containing 10.5% Si at cooling rates 4×10^2–10^6 K s^{-1} we have $A = 47(\pm 6)$, m (K s$^{-1/3}$), $n = 0.33$ (± 0.01) [4]. The measurements of distances between the dendrites in various parts of the melted zone were carried out by the installation Epiquant. The results of the measurements, as well as the calculated values of the cooling rate W, growth rate R and temperature gradient G for the alloy Al25 are presented in Table II. The values of the crystallization parameters for the laser–arc treatment lie in the range of values achieved at the laser treatment.

3.2. Silicon-phase morphology

The morphology of the silicon phase was investigated by scanning electron microscopy (SEM) after deep etching of the samples in a special reagent by the method described in [5]. After the arc-supported laser treatment, the morphology of silicon undergoes the most significant change in the alloy V124 (Fig. 4). Before treatment, the silicon crystals have the form of mutually connected plates that in the plane of the microsection are revealed as separate alien inclusions, in the aluminium matrix, as seen under the light microscope. After fusion, the silicon is precipitated around α-phase dendrites and has a fibrous structure characteristic of modified alloys. Analogous changes in morphology were observed in the directionally crystallized alloys Al–Si [6, 7]. At low crystallization rates, the lamellar silicon crystals grow owing to the twin plane re-entrant edge mechanism. The increase in the crystallization rate up to 1.26 mm s^{-1} [7] leads to a significant decrease of the twin quantity, and the author supposes that the generation of fibrous silicon crystals is connected with the transition to the continuous growth mechanism. Our TEM investigations of thin foils cut out of the surface layer of the solidified melt zone of the alloy V124 (PREM-200) showed almost total absence of twins. In our experiments the rate of the growth (Table II) exceeded the critical rates indicated in [7], therefore we may assume an analogous change in the growth mechanism at the formation of fibrous silicon crystals at the arc-supported laser fusion.

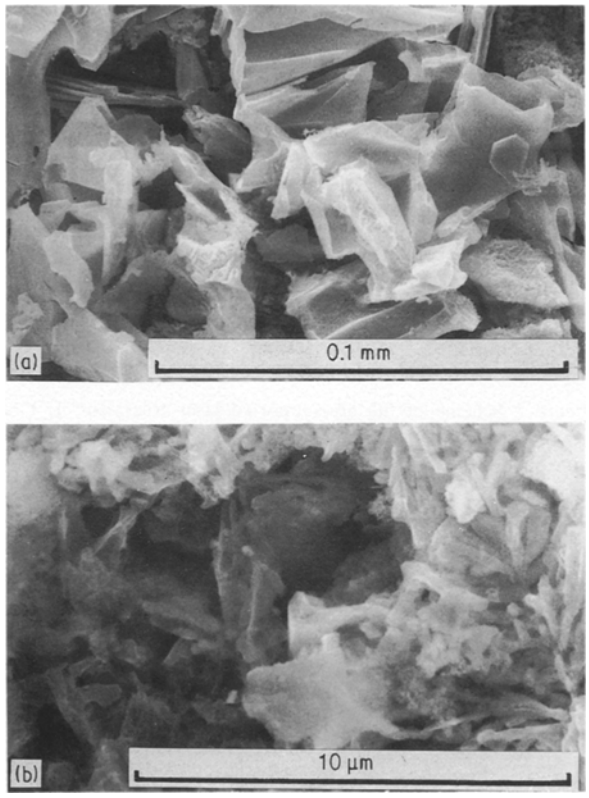

Figure 4 Morphology of silicon crystals in the alloy V124 before (a) and after (b) laser–arc treatment.

3.3. Microhardness and arc stability

The experiments on the surface fusion of alloys Al25 and V124 by arc hardening ($I = 50$–70A, $IU = 0.75$–1.00 kW) at low linear velocities of the sample movement showed that the presence or absence of the additional effect of the laser source does not significantly influence the structure, form and sizes of the solidified melt zone. The microhardness values achieved with the arc-supported laser treatment do not exceed the values achieved with treatment only by arc hardening.

Investigations on the influence of treatment rate on the microhardness and sizes of the hardened zone, and also the experiments on arc stabilization in the laser–arc treatment, were carried out at the station with the laser Latus-31, using cylindrical samples. The treatment by arc over a wide range of linear velocities of the sample movement (from 8 to 200 mm s^{-1}) showed that the velocity increase does not lead to a significant increase in microhardness (Fig. 5a). At the laser–arc fusion, a more pronounced dependence of microhardness on treatment rate is observed. Thus at the rate of ~ 133 mm s^{-1}, microhardness increases up to 175 kg mm^{-2} (Fig. 5b). Apparently, this is connected with the increase in cooling rate during the treatment by a more concentrated energy source. The increase in concentration of the laser–arc source at high linear velocities of sample movement is verified by a significant decrease of the passage width in comparison to the treatment by the arc only. Thus, while at the velocity of ~ 8 mm s^{-1} the passage width is 2.52 mm in the case of the arc treatment only, and for the combined laser–arc treatment is equal to 2.91 mm, then by increasing the velocity up to ~ 133 mm s^{-1} the opposite is obtained: the passage width is equal to

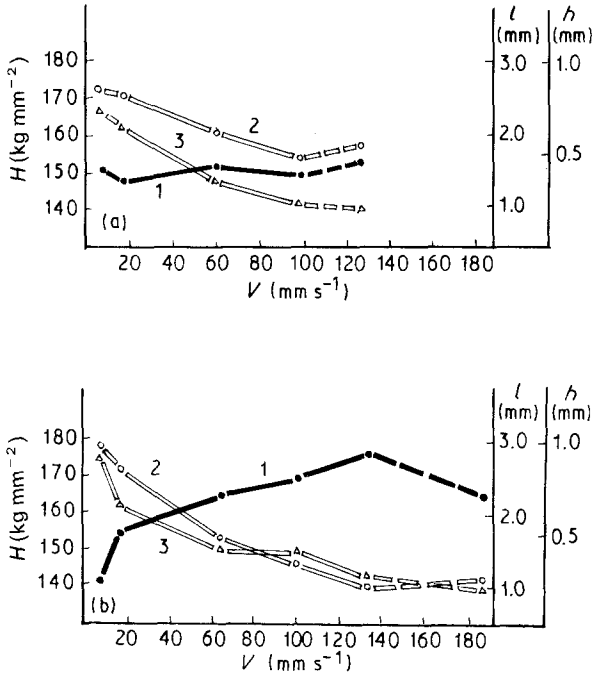

Figure 5 Dependence of the microhardness H_{50} (1), width l (2) and depth h (3) of the melted zone upon the rate of treatment by the arc (a) and the laser–arc (b) sources. $I = 70$ A. Dotted lines correspond to treatment rates with partial instability of the arc.

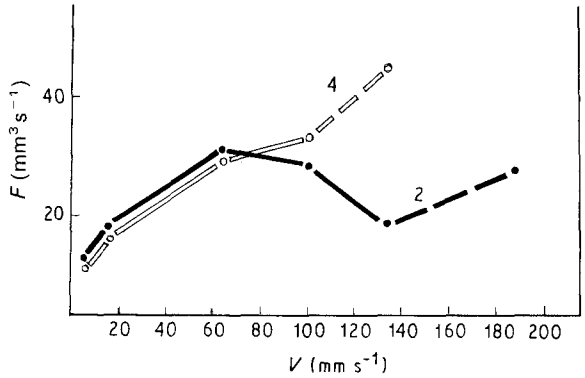

Figure 6 Rate of remelting, F, as a function of the treatment rate by the arc (1) and laser–arc (2) sources. $I = 70$ A.

1.65 mm for the arc source and 1.00 mm for the combined laser–arc source. The increase in concentration of the thermal source with the increasing treatment rate leads to a peak on the curve in Fig. 6 showing the dependence of remelting rate on treatment rate with laser–arc influence (at the arc fusion this dependence is of a monotonous character).

It should be noted that an important limitation of the arc-source application is its instability, appearing as treatment rate increases. At low surface velocities, there is a smooth fused track after the arc influence. With an increase in treatment rate the arc begins to make loops and pulsations occur. The periodic upset of the arc leads to the formation of a track consisting of separate fused sections instead of the continuous layer at the surface. Such instability at a current of 70 A is observed at the treatment rate of ~ 133 mm s^{-1}. The joined laser and arc action leads to a shift of the instability threshold in the direction of the higher rates (~ 183 mm s^{-1}). At the current value of 50 A, the arc instability appears at the treatment rate of ~ 88 mm s^{-1} and the instability of the laser–arc source appears at a rate of ~ 177 mm s^{-1}.

Thus the results above confirm the existence of optimum regimes for aluminium alloy treatment by the laser–arc source.

4. Conclusions

As a result of the investigations carried out, the optimum parameters of the laser–arc treatment of the aluminium alloys V124 and Al25 are determined. It is shown that at treatment rates up to ~ 17 mm s^{-1}, the laser–arc source and the arc source are identical in effect. At treatment rates over 17 mm s^{-1}, the laser–arc source produces the maximum hardening effect.

The microstructure of the solidified melt zone is of α-phase dendrites surrounded by the eutectic Al–Si, where Si has a fibrous structure.

The crystallization parameters (W, R, G) are determined: their values lie in the range of the values obtained at laser fusion.

References

1. W. DULY, "Laser Technology and Analysis of Materials" (Mir, Moscow, 1986).

2. A. N. SAFONOV, A. G. GRIGORIANTS, N. A. MAKUSHEVA and A. V. SERGEYEV, *Electronic Treatment of Materials* **1** (1984) 26.
3. R. W. KAN and P. HAASEN (eds) "Physical Metallurgy, Vol. 2: The phase transformations in Metals and Alloys and the Alloys with Specific Physical Properties" (Metallurgy, Moscow, 1986).
4. G. R. ARMSTRONG and H. JONES, in "Solidification and Casting of Metals: Proceedings of an International Conference on Solidification, Sheffield, 1977 (Pergamon, London, 1979) p. 454.
5. J. M. GUILLEMANY and J. M. VIRGILI, *Fundition* **32** (1986) 23.
6. R. ELLIOTT, "Eutectic Solidification Processing" (Metallurgy, Moscow, 1987).
7. O. A. ATASOY, *Z. Metallkde.* **Bd 78 H3** (1987) 177.

Received 30 October 1989
and accepted 26 October 1990